JOURNAL OF MATERIALS SCIENCE 33 (1998) 1827–1836

Solid state bonding of Al_2O_3 with Cu, Ni and Fe: characteristics and properties

L. ESPOSITO, A. BELLOSI, S. GUICCIARDI, G. DE PORTU
CNR IRTEC, National Research Council, Research Institute for Ceramics Technology, via Granarolo, 64 48018 Faenza (RA), Italy

A solid state bonding technique under hot pressing was used for joining alumina with thin metal sheets of Ni, Cu and Fe. The microstructure and microchemistry of the ceramic–metal interface and of the fracture interface were examined using scanning electron microscopy (SEM) energy dispersive spectroscopy (EDS) and X-ray diffraction (XRD), in order to identify the adhesion mechanisms and the nature of strength limiting flaws. Interaction between the selected metals and alumina can be physical or physico-chemical in nature: very low amounts of interfacial compounds were formed, depending on the processing conditions and on the presence of oxygen in the system. Fracture and toughness tests indicated that high ceramic–metal interface strengths (up to 177 MPa) were achieved under the adopted processing conditions and that strength and toughness were directly related. Moreover, an increase in hardening in the metal interlayer at a distance of 2–3 μm from the interface was observed in the samples with high strength values. The mechanical behaviour was related to several factors that strongly depend on the bonding conditions: plastic deformation of the metal, metal creep, metal intrusion and diffusion into alumina, and chemical reactions at the interface. © *1998 Chapman & Hall*

1. Introduction

The use of ceramic components in structural, electrical and electronic applications is rapidly increasing. Most of these applications require the use of ceramics bonded with metals. The performance of the resulting bonded material is influenced and often controlled by the properties (mechanical, electrical, magnetic and chemical) of the ceramic–metal interface [1–9]. The main interest in this area is therefore to develop a fundamental understanding of the parameters that control the properties of the interface, mainly governed by the specific physico-chemical interaction of the two materials [10, 11].

Chemical reactions occurring at the interface between the ceramic and the metal during bonding may lead to the formation of new phases, that eventually may influence the overall properties of the new component [3, 10]. Moreover, thermal expansion mismatch between the ceramic and the metal produces interfacial residual stresses during processing that influences the final mechanical strength of the metal–ceramic bond [8, 11].

Solid-state diffusion bonding is a joining process in which the surfaces of the two materials are held together for a certain time below the melting point of the less refractory material [2–5, 8, 12, 13]. Adherence between dissimilar phases results from atomic and molecular interactions at the interface. These interactions derive from the differences in co-ordination between the atoms at the surface (asymmetrically co-ordinated) and those in the bulk (symmetrically co-ordinated) of the material: atoms at the surface present an excess of energy, that is particularly high for metals. As a consequence in ceramic–metal joining processes the metal surface energy produces a strong driving force for shape changes that reduce the non-contacting area and for chemical changes that lower the surface energy [3, 7, 9].

The surface conditions of the sample, flatness, roughness and cleanliness, play a key role during the diffusion bonding process. Bonding temperature, pressure and atmosphere are other important variables of this joining process [8]. A wide range of metals can be bonded to single-phase and polyphase ceramics [2, 8, 9, 14–20].

The mechanisms involved in diffusion bonding are similar to those occurring in pressure sintering and they can be divided in two principal steps.

1. Plastic flow resulting from deformation of the original surface asperities.

2. Mass transfer and surface diffusion that involve the elimination of interfacial voids; at the same time an adhesion process giving the interface boundary strength also occurs.

A possible third step involves chemical reactions between the two materials and formation of new phases at the interface. The occurrence of these reactions depends on the bonding conditions (temperature, time, atmosphere and pressure) and on the chemical composition of the materials involved [6, 9]. Depending on the system, these reactions can be deleterious or, to the contrary, can lead to the

development of strong joints. In both cases the processing atmosphere plays a key role: different behaviours of metals in relation to joining properties have been found and models of ceramic interfaces have been developed in order to predict the optimum atmospheric conditions for a particular system [8, 9, 20–22]. The application of new experimental and theoretical methods has improved the understanding of the electronic structure and chemical reactions at ceramic–metal interfaces [23–29].

Mechanical characterization of a ceramic–metal joint is a complex problem and the fracture mechanisms at the interface are poorly understood [6, 8, 25–27].

In this paper, interfacial microstructures realized under different solid state bonding conditions for three ceramic–metal couples (Al_2O_3–Ni, –Cu and –Fe) are compared and related to the mechanical properties: fracture strength, fracture toughness and hardness profiles.

2. Experimental procedure

Alumina samples (96% purity) were produced starting from a commercial powder (M-KMS 96, Martinswerk). Green cold isostatically pressed bodies were sintered at 1650 °C for 1 h and the final relative density was about 96%. About 6 wt % $MgAl_2O_3$ is present, as a secondary crystalline phase. The alumina linear expansion coefficient is $8 \times 10^{-6} K^{-1}$. The flexural strength of these specimens is 226 ± 15 MPa. After sintering the dense sample, discs of 35 mm diameter and 5 mm thickness, were ground flat, polished up to 1 μm with diamond paste, cleaned in boiling water with 40 vol % nitric acid for 10 min and, finally, were annealed in air at 1000 °C for 10 min, for complete removal of the organic contaminants.

Metal foils of Cu, Ni and Fe, with a thickness of 50 μm were used. Table I shows the main characteristics of the metals. Discs of 35 mm diameter were cut and cleaned with three subsequent decreasing batches of tricloroethylene, isopropanol and ethanol, 10 min each.

Bonding cycles were performed under vacuum (10^{-1} MPa) using a hot press furnace; samples were placed in a boron nitride-lined graphite die. A pressure of 50 MPa was applied when the fixed joining temperature was reached and removed before cooling. Joining temperatures, chosen in the range 90–94% of the metal melting temperature, were: 1025 °C for the system Al_2O_3–Cu (sample ALCU), 1330 and 1350 °C for the system Al_2O_3–Ni (samples ALNI1 and ALNI2) and 1375 °C for the system Al_2O_3–Fe (sample ALFE). Table II shows the processing conditions and the characteristics of the joints.

Scanning electron microscopy (SEM) and quantitative-energy-dispersive (EDS spectroscopy) analyses, using pure elements as references (metallographically prepared in the same way as the samples) were carried out on polished cross-sections cut perpendicular to the interfaces in order to evaluate the morphology and microchemistry of the interfaces and diffusion phenomena. Moreover, as failure often occurred along the ceramic–metal interface, the two halves of the fracture surface were mounted adjacent to one another, so that equivalent locations on the metal and ceramic sides of the fracture surface were in positions of mirror symmetry. Flaws and microstructures of matching positions on the two surfaces were thus identified readily.

X-ray diffraction (XRD) analyses were carried out on the bond surfaces of metal and alumina. In particular samples ALNI2 and ALCU were analysed on the metal side, after steps of subsequent polishing until the metal layer was thin enough to allow the detectability of crystlline phases at the interface.

TABLE I Characteristics and properties of the metal foils

Metal	Purity (%)	Melting point (°C)	Boiling point (°C)	Density at 20 °C ($g\,cm^{-3}$)	Linear exp. coeff. at 0–100 °C [a] (K^{-1})	Young's modulus (GPa)
Ni	99.0	1453	2732	8.90	13.3×10^{-6}	199.5
Cu	99.9	1083	2567	8.96	17.0×10^{-6}	129.8
Fe	99.5	1535	2750	7.87	12.1×10^{-6}	211.4

[a] Linear expansion coefficient of alumina is $8 \times 10^{-6} (K^{-1})$.

TABLE II Joining conditions and mechanical properties of the tested Al_2O_3–metal couples (the pressure applied during hot pressing is 50 MPa)

Sample	System	Joining temperature (°C)	Joining temperature–metal melting temperature (%)	Joining time (min)	Flexural strength[a] (MPa)	Fracture toughness[a] ($MPa\,m^{-1/2}$)
ALNI1	Al_2O_3–Ni–Al_2O_3	1330	91.7	20	73 (13)	1.59 (0.61)
ALNI2	Al_2O_3–Ni–Al_2O_3	1350	92.9	30	149 (16)	3.70 (0.16)
ALCU	Al_2O_3–Cu–Al_2O_3	1025	94.6	15	177 (13)	2.24 (1.56)
ALFE	Al_2O_3–Fe–Al_2O_3	1375	89.4	2	50 (11)	0.83 (0.12)

[a] Values in brackets are the standard deviations.

The fracture strength of the joints was evaluated in three-point bending on bars $14.0 \times 2.0 \times 1.5$ mm, length × width × thickness, respectively, on an 11 mm span with a crosshead speed of 0.5 mm min^{-1}, as sketched in Fig. 1. The fracture strength was calculated with the usual bending formula. Fracture toughness, K_{Ic}, was evaluated by the single edge notched beam (SENB) method in three-point bending. In bars of $14 \times 2 \times 3$ mm, length × width × thickness, respectively, a notch, 140 μm wide and 1 mm deep, was carefully introduced with a diamond saw in correspondence with the metal foil, as shown in Fig. 2. The bars were then broken on an 11 mm span with a crosshead speed of 0.05 mm min^{-1}. The values of fracture toughness were calculated assuming that the bars were made of a monolithic material, according to [30]

$$K_{Ic} = y\frac{3sP}{2bd^2}10^{-6}(\pi c)^{1/2} \quad (1)$$

where K_{Ic} was the fracture toughness (MPa m$^{-1/2}$), y the shape factor; s the span (metres); P the fracture load (Newtons); b and d the width (metres) and the thickness (metres) of the bar, respectively; and c the depth of the notch (metres). The authors are aware that to evaluate the fracture toughness of an interface between dissimilar materials a much more complex analysis and specific experimental set up would be required [31]. Nevertheless, our main intention was to compare different systems more than evaluating *per se* the fracture toughness of the interface.

Using a very "local probe", hardness tests were carried out on a cross-section of the metal–ceramic interface to see if some effects due to interaction between the ceramic and the metal could be detected. Knoop microhardness profiles were made using a Zwick 3212 hardness tester. Knoop microhardness was measured with a load of 0.0981 N in the metal foil as a function of the distance to the interface between alumina and metal, as shown in Fig. 3. The major diagonal of the indentation was held parallel to the interface and the distance was taken as the distance between the interface and the centre of the indentation.

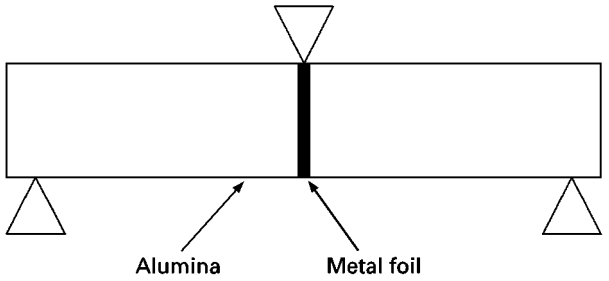

Figure 1 Schematic of the three-point flexural test for the determination of bond strength.

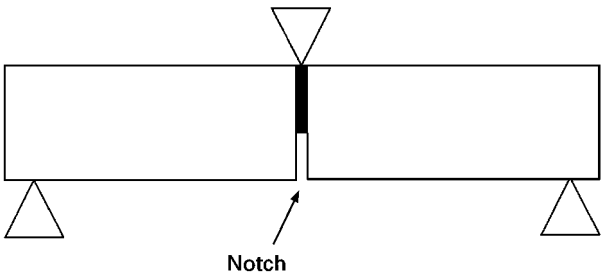

Figure 2 Schematic of the SENB three-point flexural test for the determination of bond toughness.

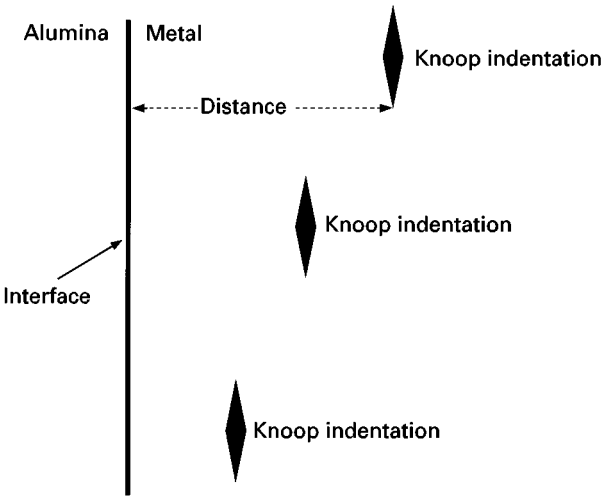

Figure 3 Knoop hardness indentations at decreasing distance from the metal–alumina interface for construction of the microhardness profile.

3. Results and discussion

3.1. Microstructure

The microstructure and microchemistry of polished cross-sections cut perpendicular to the planes of the joining interfaces are shown in Figs 4 (ALNI2), 5 (ALCU) and 6 (ALFE).

In all three cases, the metal foil adheres to the ceramic and fills up the pores in the surface. In samples ALNI1, ALNI2 and ALCU the presence of metal inside the alumina pores was detected up to a depth of about 10 μm from the interface. In sample ALFE the metal was present only inside pores at the surface. The uniaxial pressure applied was responsible for a slight decrease in thickness in the metal layer.

Solid state bonding works primarily through deformation of the metallic foil as a consequence of the combined effects of applied pressure and temperature, leading to intimate contact between the two materials. This phenomenon is strongly influenced by the roughness of the alumina. In the first stage of the process, the real contact area is smaller than the total surface area as pores are present at the interfaces. It has been hypothesized that contact growth is governed by vacancy diffusion in the metal, so that the pores at the interface disappear [15].

Because metal creep cannot sufficiently fill up all the cavities remaining after polishing, a diffusion process may lead to enhanced filling of the cavities under specific conditions of temperature and time. Evaporation–condensation phenomena have been hypothesized [25] to allow interfacial diffusion, particularly for subsurface pores.

Fig. 7a, b (secondary electron and back scattered electron images, respectively) show the ceramic and

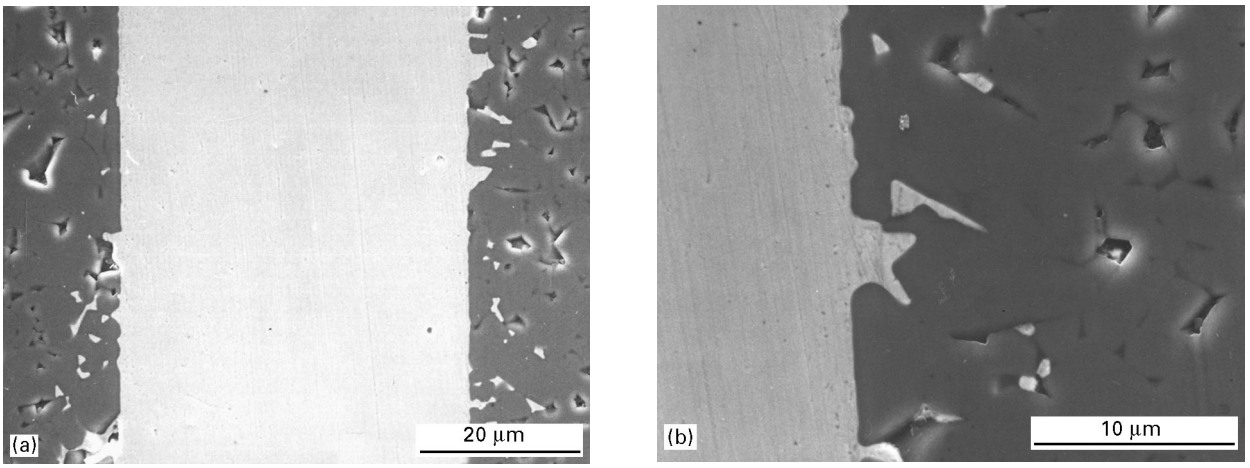

Figure 4 Sample ALNI2: SEM image of the polished cross-section perpendicular to the interface.

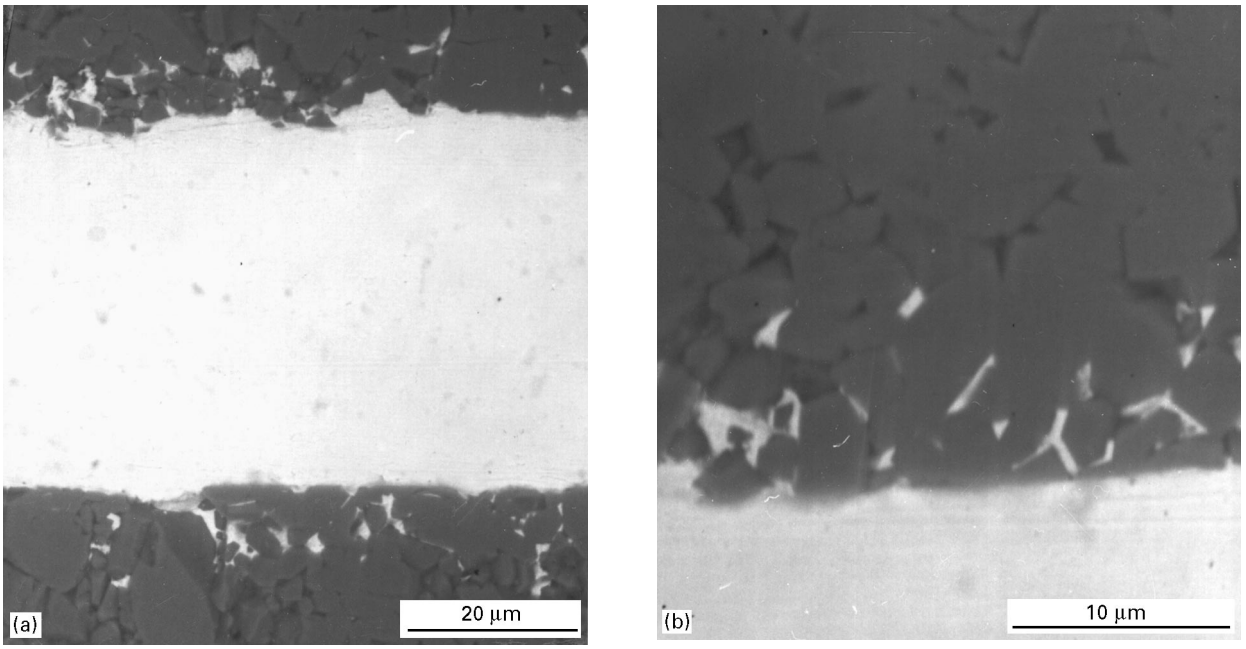

Figure 5 Sample ALCU: SEM image of the polished cross-section perpendicular to the interface.

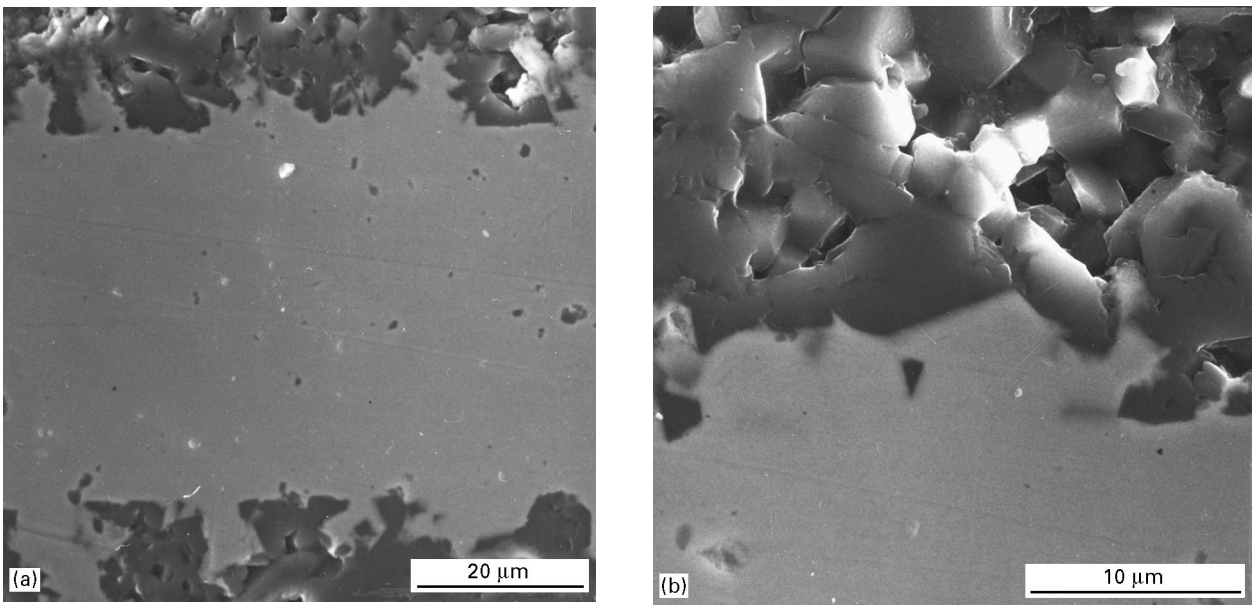

Figure 6 Sample ALFE: SEM image of the polished cross-section perpendicular to the interface.

metal sides of the fracture surface of sample ALCU. Similar microstructures can also be observed for the other samples. The images illustrate the grain imprints from the metal side and their corresponding locations on the ceramic side. Good contact along the ceramic–metal interface was achieved and maintained during bonding. On the metal side, regions where ceramic grain-boundary imprints are absent can also be observed. Regions where no contact was produced seem to be associated with the presence of cavities on the surface of the ceramic.

Reactions occurring at the interface affect the properties of the resulting products. As Al_2O_3 represents a state of high thermal stability, the formation of strong bonds with metals requires elemental diffusion form metal to ceramic. Reactions between metal and Al_2O_3 strongly depend on temperature, time and atmosphere. Under the adopted experimental conditions chemical reactions are likely to occur between the metal and Al_2O_3.

The microstructural and chemical analyses performed on the tested samples are described in the following paragraphs. Hypotheses about possible macroscopic reactions and about the reaction mechanisms occurring at the interface during joining are suggested and thermodynamic calculations are also reported for each Al_2O_3–metal system.

3.1.1. The Al_2O_3–Ni system

Fig. 8a and b show the morphology and X-ray map of Ni at the Al_2O_3-Ni interface of sample ALNI2. A slight Ni diffusion in Al_2O_3 was also observed in sample ALNI1. Elements present in the ceramic part (Al, O, Mg, Si) do not diffuse into the metal. Nickel is present in large amounts within the pores; it is also diffused for about 15 μm from the interface in the Al_2O_3 bulk. In order to quantify the amount of Ni diffused into Al_2O_3 several spot analyses were conducted at the same distance from the interface. These analyses show that the nickel content decreases steadily from the interface to about 15 μm into the alumina bulk and is higher in sample ALNI2 ($\sim$ 1 wt %) than in ALNI1 ($\sim$0.7 wt %). Therefore, the bonding temperature seems to influence the diffusion rate, as expected, because an increase of the bonding temperature of 20 °C between ALNI1 and ALNI2 induces higher Ni diffusion in Al_2O_3. This behaviour

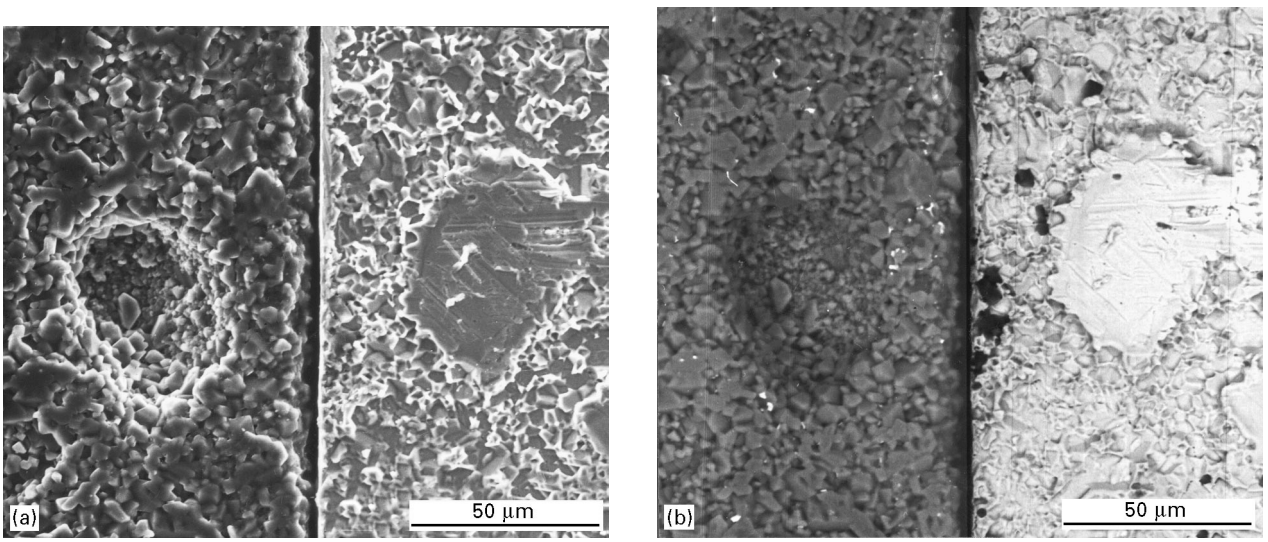

Figure 7 Sample ALCU: SEM specular images of the ceramic (left) and metal (right) side of the fracture surface. (a) Secondary electron image, and (b) back scattered electron image.

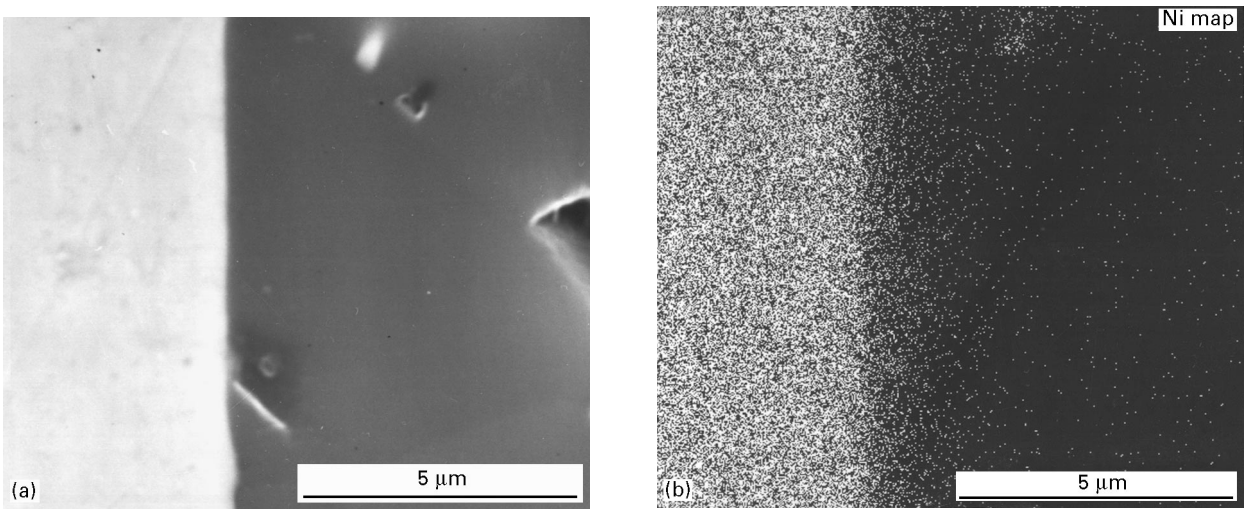

Figure 8 Sample ALNI2: morphology (a) and nickel X-ray map (b) at the Al_2O_3–Ni interface.

is in agreement with previous results [32] conducted on the system NiO–Al_2O_3 (it can be considered similar to the Ni–Al_2O_3 system because of the presence of a thin NiO layer at the Ni surface) in which the reaction between NiO and Al_2O_3 was shown to be controlled by Ni–Al interdiffusion. Moreover, Hirota and Komatsu [33] have shown that diffusion occurs preferentially through the alumina bulk rather than along the grain boundaries.

For the XRD analyses, the ALNI2 joint was fractured along the ceramic–metal interface. X-ray analysis of these surfaces did not reveal any crystalline phase besides the expected ones: Al_2O_3, $MgAl_2O_4$ and Ni. For a deeper analysis, the metal surface was then polished, in steps of 5 μm each. X-ray analysis was performed after each step. In this way the presence of a low amount of $NiO \cdot 5Al_2O_3$ was clearly detected just before complete removal of the Ni layer.

Numerous studies have analysed the Al_2O_3–Ni system both experimentally and thermodynamically. The spinel $NiAl_2O_4$ has often been found as an interphase. The reaction mechanism generally suggested for its formation involves an NiO intermediate [12]

$$\langle Al_2O_3 \rangle + \langle NiO \rangle \Rightarrow \langle NiAl_2O_4 \rangle \quad (2)$$

with an associated free energy change of $\Delta G = -6000 - 9.5 \times T$ (J mol^{-1}) [34], where T is the temperature.

Under the adopted experimental conditions this spinel phase should form. However, as only $NiO \cdot 5Al_2O_3$ was found, its formation instead of the spinel phase (whether or not it passed through the NiO intermediate) was supposed to be a consequence of the uniaxial pressure (50 MPa) used during the joining cycle: that changed the thermodynamic equilibrium of the system, leading to the formation of a more alumina-rich phase.

The oxygen involved in $NiO \cdot 5Al_2O_3$ formation could come from Ni, where it was dissolved in low amounts and/or from the furnace atmosphere. From a thermodynamic point of view, we can expect a contribution from the oxygen present in the chamber as the reaction

$$2\langle Ni \rangle + (O_2) \Rightarrow 2\langle NiO \rangle \quad (3)$$

is associated with a negative free energy change of $\Delta G^{\circ}_{1350\,^{\circ}C} = -173\,000$ (J mol^{-1}) [34]; the equilibrium oxygen partial pressure P_{O_2}, for this reaction calculated from

$$\Delta G = \Delta G^0 - \text{r.t.} \times \ln P_{O_2} = 0 \quad (4)$$

is equal to 2.7×10^{-6} Pa, where r. is the gas constant and t. the temperature. Because the vacuum in the chamber is only 10^{-1} Pa, Ni oxidation could occur. This would require that the oxygen coming from the chamber atmosphere and diffusing into nickel or along the interface reacts preferentially at the edges of the bond. On the contrary, microscopic analyses did not show any difference in the morphology and composition of the interface between the central and edge parts of the sample. Consequently the oxygen involved in the chemical reaction is supposed to come from the nickel.

This oxygen source has also been hypothesized by Trumble and Rühle [35], who suggested that the formation of a spinel-type phase does not necessarily occur through an NiO intermediate, but that it is mainly influenced by the critical oxygen activity that increases with temperature. According to this reaction mechanism, the oxygen source may be the oxygen initially dissolved in the Ni and not the residual one in the atmosphere of the chamber, the calculated critical oxygen required for nickel aluminate formation was shown to be much lower than the solubility limit of oxygen in Ni [35].

Moreover, no reaction layer was found between Al_2O_3 and Ni; therefore, the reaction products were present in very low amounts and randomly located on the surface of the Al_2O_3 grains at the interface. The ceramic part of the fractured interface of sample ALNI2 shows the presence of flakes of Ni-rich phase within the grain boundaries (Fig. 9a, b). In some areas, on the surface of the Al_2O_3 grains, the formation of phases within the Ni–Al–O system can also be observed. The same interfacial as reactions are supposed to occur also in sample ALNI1, but in a smaller amount because the processing temperature is lower.

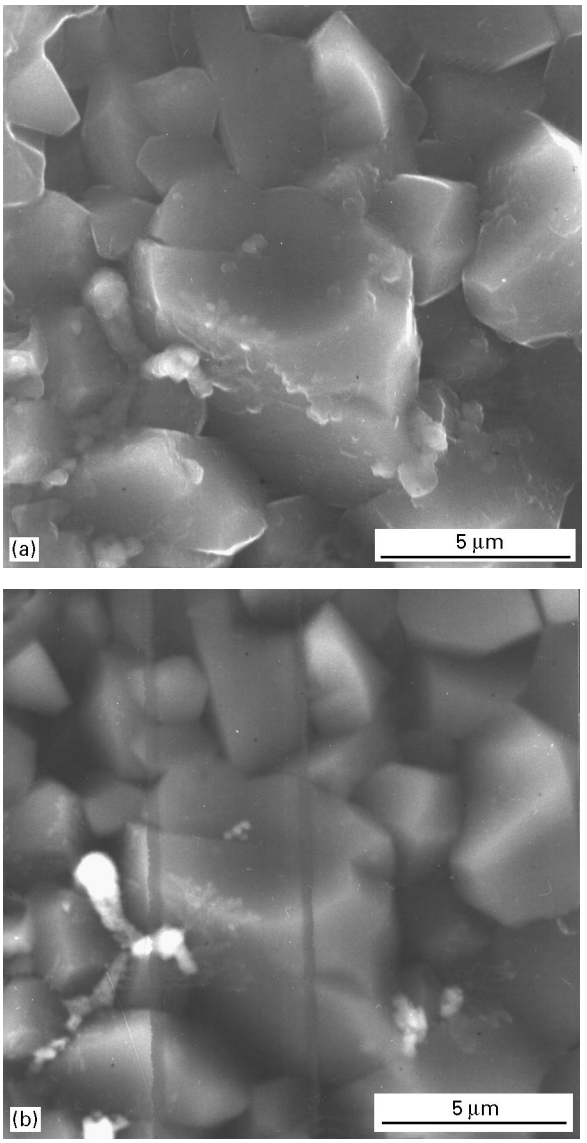

Figure 9 Sample ALNI2: ceramic side of the fracture surface at the interface between Al_2O_3 and nickel. (a) Secondary electron image, and (b) back scattered electron image.

3.1.2. The Al_2O_3–Cu system

Cu diffusion up to about 1 wt % occurred to a depth of about 15 μm from the interface in the Al_2O_3 bulk. The presence of traces of Al and O in the metal seems to be associated with the presence of Al_2O_3 grains, which probably entered the bulk of the Cu during its deformation under pressure.

No new crystalline phase was identified at the interface probably because of the limited amount of Cu. In particular, the phase $CuAl_2O_4$, which probably formed from reaction between CuO and Al_2O_3, was difficult to detect because it has the same spinel type structure and consequently the same XRD peak positions as the phase $MgAl_2O_4$, already present in the Al_2O_3 bulk as a secondary phase. The possibility of a thin (few nanometers) amorphous reaction film, previously observed [25], cannot be excluded in view of the sensitivity of the analytical method used. Therefore, a Cu–Al–O phase (probably $CuAlO_2$ or $CuAl_2O_4$) is likely to be present. Its formation may be correlated either with the slight oxidation of Cu, owing to the low level of vacuum inside the furnace, or to the oxygen dissolved in copper. In the latter case, a reaction mechanism similar to the one described for the system Al_2O_3–Ni can be suggested. In any case the reaction proceeds either through a copper oxide intermediate (CuO or Cu_2O) or directly [23, 27, 34]

$$\langle CuO\rangle + \langle Al_2O_3\rangle \Rightarrow \langle CuAl_2O_4\rangle \quad (5)$$

$$\Delta G = -110\,000 + 8.5 \times T \ (J\,mol^{-1})$$

$$\langle Cu\rangle + 1/2(O_2) + \langle Al_2O_3\rangle \Rightarrow \langle CuAl_2O_4\rangle \quad (6)$$

$$\Delta G = -272\,000 + 83.5 \times T \ (J\,mol^{-1})$$

Calculations [36] of P_{O_2} equilibrium in the reported reactions and of other possible ones that are energetically favoured, show that P_{O_2} is always lower in the chamber, consequently, the formation of a spinel-type phase or of other Cu–Al–O based phases is thermodynamically favoured. Naidich [37] and Chatain *et al.* [38] have suggested that oxygen influences the copper wetting behaviour through the formation of oxygen–copper clusters that segregate at the interface. The occurrence of similar oxygen clustering and segregation in solid copper should also affect the interfacial characteristics [34].

On the ceramic side of the fracture interface of our sample (Fig. 10a, b), Al_2O_3 in contact with copper contains some small particles (about 1–5 μm) of Cu that have partially reacted with alumina inside the grain boundaries. On the metal side (Fig. 11a, b), some Al_2O_3 grains are attached to copper, showing pull-out during propagation of the fracture.

The good adhesion (described in Section 3.2) obtained in this sample can be correlated not only with the possible presence at the interface of a reaction compound, but also with the diffusion of copper into alumina. Consequently, a bonding mechanism similar to the one described for the system ALNI2 can also be hypothesized for sample ALCU. Other authors [27] have considered a similar behaviour of nickel and copper bonded to alumina.

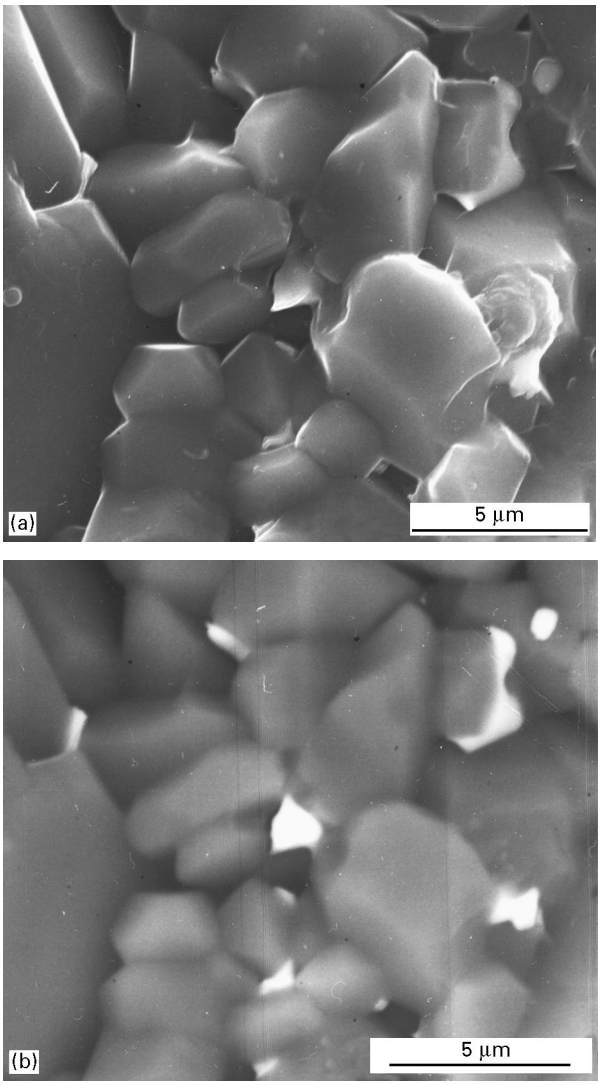

Figure 10 Sample ALCU: ceramic side of the fracture surface at the interface between Al_2O_3 and copper. (a) Secondary electron image, and (b) back scattered electron image.

3.1.3. The Al_2O_3–Fe system

The characteristics of the interface are similar to the other systems: oxygen and aluminium are absent in the metal part and slight diffusion of iron up to 5–10 μm in the bulk of Al_2O_3 occurs.

The amount of iron in the alumina detected by EDS is 0.5 wt % up to 5–8 μm from the interface. In this sample less adhesion was obtained (see Section 3.2) compared with ALNI and ALCU. It was probably caused by the lower iron diffusion into alumina. The joining time of only 2 min (compare the processing parameters in Table II) limited iron diffusion. No reaction layer was observed with the back scattered SEM analysis and, in addition, no reaction products at the interface were detected by XRD. As previously suggested [3], bridging of oxygen ions can be considered to be responsible for bond formation in the Al_2O_3–Fe system, in addition to physical bonds.

3.2. Mechanical properties

In Table II, the mean values and the standard deviations of flexural strength and fracture toughness are reported.

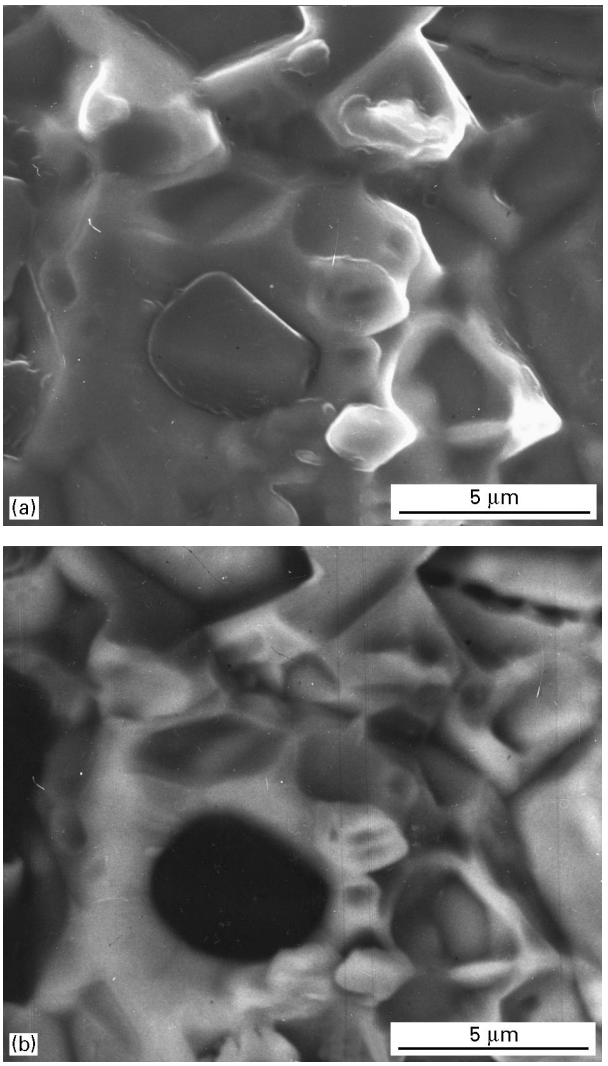

Figure 11 Sample ALCU: metal side of the fracture surface at the interface between Al_2O_3 and copper. (a) Secondary electron image, and (b) back scattered electron image.

Save for two fracture toughness specimens, all the specimens broke with a linear load–deflection curve at the ceramic–metal interface. The absence of any effect such as plastic deformation could be due to the low thickness of the metal foil. As the joining interface was the weak point for all the ceramic–metal systems, the values of flexural strength and fracture toughness reported in Table II can permit some consideration about the mechanical behaviour of the joint.

Samples ALFE and ALNI1 show poor mechanical strengths when compared with ALCU and ALNI2. In the system Al_2O_3–Ni, the bonding temperature seems to be a crucial aspect: the increase in the bonding temperature of 20 °C (Table II), nearly doubled the values of flexural strength and fracture toughness. In this system, the change in flexural strength seems to be proportional directly to the change in fracture toughness, suggesting a behaviour that can be related to the Griffith theory [39]. If the system ceramic–metal–ceramic is considered as a homogeneous material, then the fracture is initiated at the point of pre-existing critical defects, as in normal brittle material. In our systems, such pre-existing critical defects are residual porosity or unbonded zones at the interfaces similar to those shown in Fig. 7a, b and described also in previous studies [31]. In the system ALCU the high flexural strength, when compared with its relatively low fracture toughness, could indicate the presence of small critical defects. However, in this system, two SENB specimens gave very low values (see the standard deviation in Table II) while the other two specimens had fracture toughness values close to 4 MPa $m^{1/2}$. It is likely that preparation for the SENB tests damaged the two low-value bars. The high flexural strength and the high fracture toughness of the ALCU and ALNI2 systems indicate that the bonding conditions have promoted strong adhesion between the ceramic and the metal. Good bonding is often associated with an interface reaction phase. In sample ALNI2, the presence of the phase $NiO \cdot 5Al_2O_3$ has a positive effect on strength; by contrast, the presence of the spinel nickel aluminate was previously found to be damaging to the strength of the interface [37]. Consequently, the use of uniaxial pressure during the joining cycle favours the formation at the interface of an alumina-rich phase, whose physical and chemical characteristics have a positive effect on the strength of the joining.

Beside the microstructure and microchemistry of the interface, other features have a strong effect on the mechanical behaviour of Al_2O_3–metal couples. The flexural strength of the metal–ceramic bond has been reported [40] to be proportional inversely to the thermal expansion coefficient of the metal. In those experiments, the metal–alumina bond was obtained *via* the insert of an additional aluminium foil between metal and ceramic. Strong residual tension stresses and the formation of brittle intermetallic layers were indicated as the major causes responsible for strength degradation. Instead, in the present case, the metal is directly bonded to the alumina and, except for sample ALNI1, which was processed at a temperature too low for solid state bonding, the flexural strength shows a direct, albeit non-linear, correlation with the thermal expansion coefficient of the metal (Fig. 12): the higher the thermal expansion of the metal, the stronger the bond (Tables I and II). The high residual thermal stresses can be roughly estimated by the following relation [8]

$$\sigma_{res} = \frac{E_i E_j}{E_i + E_j}(\alpha_i - \alpha_j)\Delta T \qquad (7)$$

where σ_{res} is the residual thermal stress, E is Young's modulus, α the thermal expansion coefficient, ΔT the temperature cooling range, and i and j refer to the materials being bonded. According to Equation 7 by inserting the data reported in Table II the residual stresses calculated and the processing parameters (namely ΔT) are 906, 864 and 738 MPa for ALNI2, ALCU and ALFE, respectively. These values largely exceed the yield strengths of the metals (145, 69 and 200 MPa for nickel, copper and iron, respectively [41]). Some plastic deformation, which relieves the strong residual stress at the interface, can, therefore, be expected. While it is very difficult to model the residual plastic stress and its influence on the bond strength [8], in our case, flexural strength seems to be related inversely to yield strength of the metal as shown in Fig. 13.

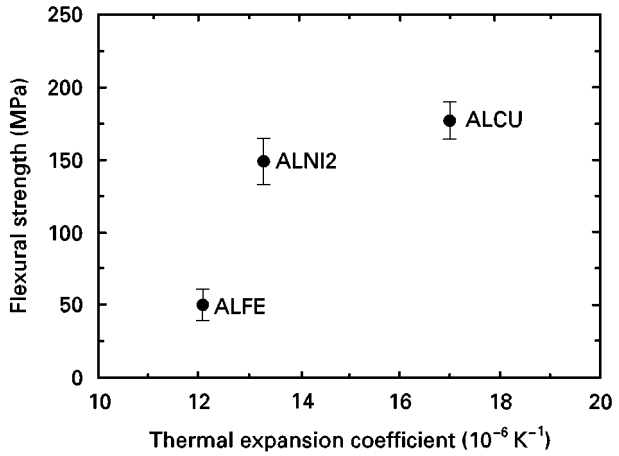

Figure 12 Flexural strength as a function of the linear thermal expansion coefficient of the metal.

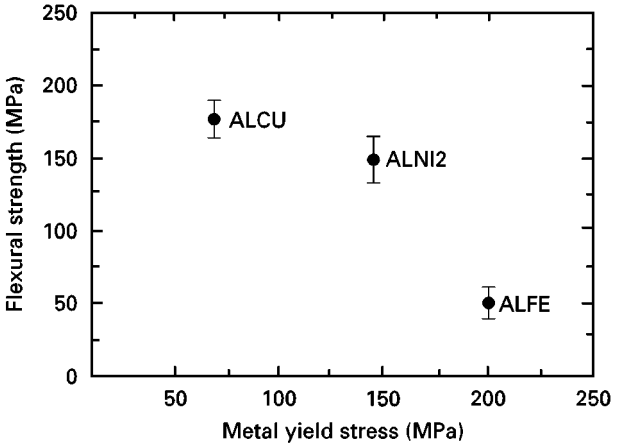

Figure 13 Flexural strength as a function of the yield stress of the metal.

The Knoop hardness profiles in metal interlayers are reported in Fig. 14. In sample ALFE, the mean hardness is roughly 1.4 GPa within a scatter band of $\pm$ 0.5 GPa and with a slight increase at a distance of less than 2 μm from the ceramic–metal interface. In system ALCU, the mean hardness is lower than that of the iron, as expected, and occurs mainly in a scatter band of $\pm$ 0.5 GPa. In this sample, the hardening phenomenon close to the interface is much more pronounced. This effect is clearly evident at a distance of less than 3 μm. In the system Al_2O_3–Ni, we measured an almost constant value of hardness in sample ALNI1. The mean value of hardness in the nickel foil is similar to that of the iron with a comparable scatter band, and no indication of hardness increase close to the interface is found. In sample ALNI2, the hardness profile in the bulk of the nickel foil has the same features as in sample ALNI1 but with a sharp increase in hardness when approaching the interface. Again, this increase is evident at a distance of less than 2–3 μm. As a general indication, it seems that the most apparent hardness increments occur in the systems with the highest flexural strength, i.e. ALCU and ALNI2 (see Table II and Fig. 14): hardness profiles seem to permit the identification of systems with the strongest adhesion between metal and ceramic.

Because of several factors (absence of diffusion from ceramic to metal, absence of mechanical effects such as residual thermal stress on plastic strain because they should be constant along the metal foil section), the reasons for the increase in hardness are not yet fully understood. This means that further studies are required. However, some plausible explanations can be proposed: (a) the occurrence of very local chemical reactions, and (b) the adhesion promoted by physical

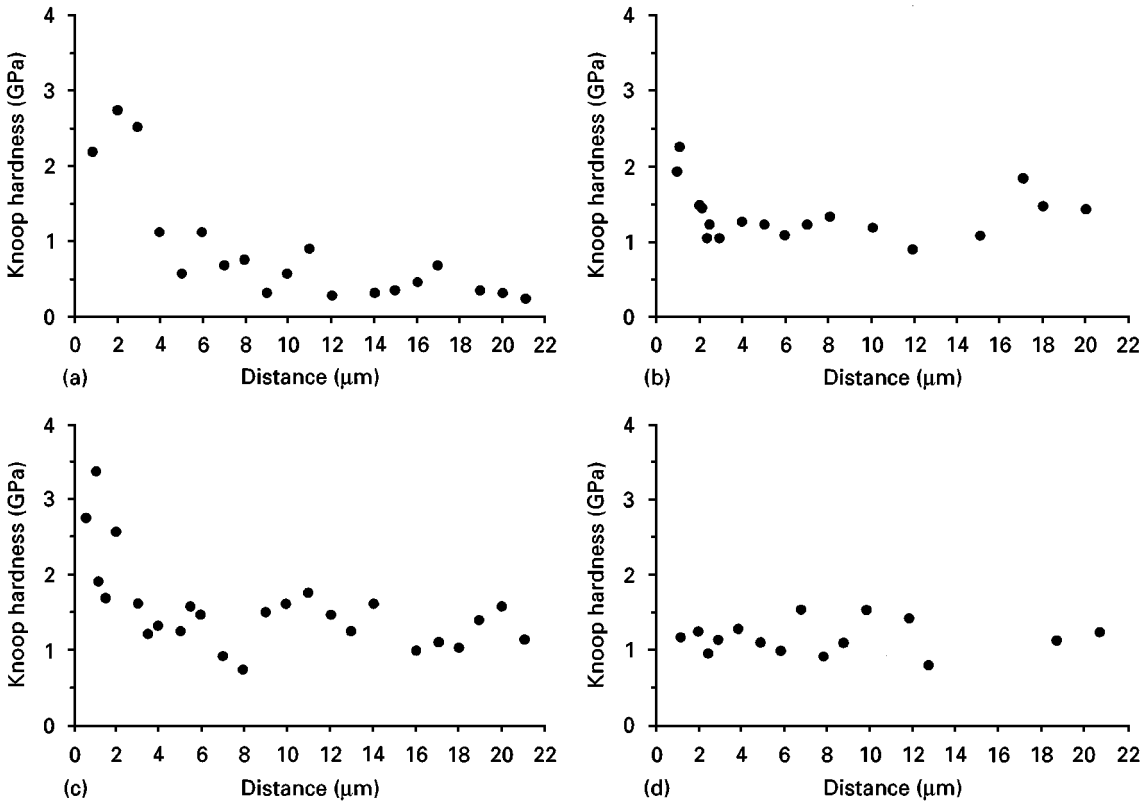

Figure 14 Metal Knoop hardness as a function of the distance from the metal–alumina interface: (a) ALCU, (b) ALFE, (c) ALNI2, and (d) ALNI1.

interactions: diffusion of metal to ceramic, metal creep, surface diffusion and metal flow. These different phenomena, associated also with surface characteristics, strongly contribute to metal–ceramic adhesion and seem to influence the hardness of the metal very close (2–3 μm) to the interface.

4. Conclusions

Alumina ceramics were joined through hot-pressing using Ni, Cu and Fe metal interlayers. The results indicate that high quality Al_2O_3–metal bonds are possible with the solid state bonding technique.

From the analyses of microstructure and microchemistry at the interface and from the proposed adhesion mechanisms, the phenomena involved can be outlined as follows: the interaction between Cu, Ni, Fe and Al_2O_3 can be physical or physico-chemical in nature. Different phenomena (plastic deformation, metal creep, surface diffusion, evaporation–condensation) act simultaneously and affect mechanical adhesion. In addition, chemical reactions occur between Al_2O_3 and the metal leading to the formation of very low amounts of interfacial compounds. In sample ALNI2, the compound $NiO \cdot 5Al_2O_3$ was found at the interface by XRD. In sample ALCU the formation at the interface of a very low amount of a spinel-type phase was hypothesized. In samples ALNI1 and ALFE, no new chemical compounds were formed at the interface. The occurrence of chemical reactions has been found to be dependent on the bonding conditions adopted (joining temperature, time and pressure) and on the presence of oxygen in the system. In particular, they are dependent on the amount of oxygen present in nickel for the sample ALNI2. In both the Cu–Al_2O_3 and Ni–Al_2O_3 systems the reaction phase is very narrow. Consequently, the occurrence of chemical reactions involved in bonding has to be determined in each individual case. Moreover, the rate-controlling mechanisms are not yet fully understood and further work is necessary in this respect.

The flexural strength of samples ALNI2 and ALCU is 149 and 177 MPa, respectively, while samples ALNI1 and ALFE present a much lower strength. A hardening increase effect observed in the metal at a distance of 2–3 μm from the interface in samples ALNI2 and ALCU was found to be connected with the higher flexural strength of these samples. The different mechanical behaviour can be related to several factors: the diffusion level of the metal into alumina, the occurrence of chemical reactions at the interface and the joining conditions.

References

1. A. P. TOMSIA, *J. Physique IV*, Colloque C7, **3** (1993) 1317.
2. B. DERBY, in "Joining of ceramics" edited by M. G. Nicholas (Chapman & Hall, London, 1990) p. 94.
3. J. T. KLOMP, *ibid.* p. 113.
4. F. S. OHUCHI and M. KOYAMA, *J. Amer Ceram. Soc.* **74** (1991) 1163.
5. A. P. TOMSIA and R. E. LOEHMAN, *Mater. Manufact. Processes* **9** (1994) 547.
6. M. BACKHAUS-RICOULT, in "Metal-ceramic interfaces", *Acta Scripta Metall., Proc. Series* Vol 4, edited by M. Rühle, A. G. Evans, M. F. Ashby and J. P. Hirth (Pergamon press, Oxford, 1990), 79.
7. M. G. NICHOLAS, in "Joining of ceramics" (Chapman & Hall, London, 1990) p. 72.
8. O. M. AKSELSEN, *J. Mater Sci.* **27** (1992) 569.
9. J. T. KLOMP, *Amer. Ceram. Bull.* **59** (1980) 794.
10. D. MUNZ and Y. Y. YANG, *J. Europ. Ceram. Soc.* **13** (1994) 453.
11. B. J. DALGLEISH, K. P. TRUMBLE and A. G. EVANS, "Metal-ceramic interfaces", *Acta Scripta Metall., Proc. Series* Vol 4, edited by M. Rühle, A. G. Evans, M. F. Ashby and J. P. Hirth (Pergamon press, Oxford, 1990), 420.
12. F. P. BAILEY and W. E. BORBIDGE, *Mater. Sci. Res.* **14** (1981) 525.
13. G. ELSSNER, in "Joining ceramics, glass and metal" (ed) H. Krappitz and H. A. Shaeffer (Verlag der Deutsche Glastechnischen Gesellschaft e. V., Frankfurt/M, 1993) p. 241.
14. W. DAWHIL and E. KLINGER, *Ber. Dtsch. Keram. Ges.* **46** (1969) 12.
15. J. T. KLOMP, in "Science of ceramics" (eds) C. Brosset and E. Knopp (Swedish Institute for Silicate Research, Gothenberg, 1970) p. 501.
16. H. J. DE BRUIN, A. F. MOODIE and C. E. WARBLE, *J. Aust. Ceram. Soc.* **7** (1971) 57.
17. E. TRESSLER, T. L. MOORE and R. L. CRANE, *J. Mater. Sci.* **8** (1971) 151.
18. A. G. BUYERS, *J. Amer Ceram. Soc.* **46** (1963) 244.
19. J. T. KLOMP, *Amer. Ceram. Soc. Bull.* **51** (1972) 683.
20. J. E. MCDONALD and J. G. EBERHART, Second International Conference of Science of Hard Materials, *Trans. Metall. Soc., AIME* **233** (1965) 512.
21. J. G. LI, *J. Mater. Sci. Lett.* **11** (1992) 803.
22. *Idem*, *ibid.* **11** (1992) 3118.
23. Y. YOSHINO, *J. Amer. Ceram. Soc.* **72** (1989) 1322.
24. M. A. MARTINEZ, J. RODRIGUEZ, C. NAVARRO, R. PORTES and V. SANCHEZ-GALVEZ, *J. Mater. Sci.* **27** (1992) 4230.
25. Y. YOSHINO and T. SHIBATA, *J. Amer. Ceram. Soc.* **75** (1992) 2756.
26. C. BERTAUD, M. COURBIERE, C. ESNOUF, D. JUVE and D. TREHEUX, *J. Mater. Sci.* **24** (1989) 4545.
27. M. L. SHALZ, B. J. DAGLEISH, A. P. TOMSIA and A. M. GLAESER, *ibid.* **28** (1993) 1673.
28. T. NAGANO and F. WAKAY, *J. Ceram. Soc. Jpn. Int. Eds* 102 (1994) 690.
29. A. G. BALOGH, M. P. MACHT and V. NAUNDORF, *J. Mater. Res.* **9** (1994) 406.
30. "Stress intensity factors handbook", Vol. 1, edited by Y. Murakami (Pergamon Press, Oxford, 1987) p. 13.
31. G. EVANS, M. RÜHLE, G J. DALGLEISH and P. G. CHARALAMBIDES, "Metal-ceramic interfaces", *Acta Scripta Metall., Proc. Series* Vol 4, edited by M. Rühle, A. G. Evans, M. F. Ashby and J. P. Hirth (Pergamon press, Oxford, 1990), 345.
32. F. S. PETTIT, E. H. RANDKLEV and E. J. FELTEN, *J. Amer Ceram. Soc.* **49** (1966) 199.
33. K. HIROTA and W. KOMATSU, *ibid.* **60** (1977) 105.
34. O. KUBASCHEWSKI, C. B. ALCOCK and P. J. SPENCER, in "Materials thermochemistry" (Pergamon Press, Oxford, 1993).
35. K. P. TRUMBLE and M. RÜHLE, *Acta Scripta Metall. Proc.* **4** (1990) 144.
36. R. AIREY, J. C. AMBROSE and M. G. NICHOLAS, in "Joining ceramics, glass and metal" (eds) H. Krappitz and H. A. Shaeffer (Königswinter Verlag der Duetschen Glastechnischen Gesellschaft, Frankfurt, 1993) p. 15.
37. Y. U. NAIDICH, *Prog. Surf. Membrane Sci.* **14** (1981) 353.
38. D. CHATAIN, L. COURDRIER and N. EUSTATHOPOULOS, *Rev. Phys. Appl.* **23** (1988) 1055.
39. A. A. GRIFFITH, *Phil. Trans. R. Soc. Lond* **A221** (1920) 163.
40. G. ELSSNER, in "Joining of ceramics" edited by M. G. Nicholas (Chapman & Hall, London, 1990) p. 128.
41. C. L. MANTELL, in "Engineering materials handbook" (McGraw-Hill, New York, 1958).

Received 11 November 1996
and accepted 5 December 1997